MODELING OF HTSC-BASED IRON CORE FLUX-CANCELING ELECTRODYNAMIC SUSPENSION FOR MAGLEV

Marc T. Thompson, Ph.D.[1]
Consultant
19 Commonwealth Road Watertown, MA 02172
(617) 923-1392
marctt@mit.edu

Richard D. Thornton, Sc.D.

Massachusetts Institute of Technology
77 Massachusetts Avenue, Room 10-050
Cambridge, MA 02139
thornton@mit.edu

Magnemotion, Inc.
142V North Road
Sudbury, MA 01776
mmi-rdt@magnemotion.com

SUMMARY

The design and analysis of a new iron core "flux-canceling" magnetic suspension suitable for high-temperature superconductors (HTSC) is described. A 1/5-scale model of this suspension has been designed and tested with a high-speed rotating wheel test facility. A new low-cost multiple-loop guideway has been tested and lift, drag, and guidance forces have been measured at operating speeds approaching that of a full-scale train. These results are compared to predictions based on simple circuit models, with good results.

A vertical control system has been designed and tested to improve ride quality through differential control of the magnet currents. The test fixture has also been used to validate the concept of lift generation at zero train velocity by AC excitation of the main magnet coils. Scaling laws have been applied to the results and predictions made for a full-scale HTSC suspension operating at 40K. Further work in this area may help overcome one of the fundamental limitations of electrodynamic (EDS) Maglev --- the fact that there is zero levitation force at zero train velocity and a low speed suspension is needed.

INTRODUCTION

Magnetic levitation for high speed ground transportation (Maglev) has been an active area of research and development for over 30 years. This new transportation mode has been proposed as an alternative to air, automobile, and high-speed train travel. Various experimental and a large number of theoretical studies have been done. Work has been continuous in Japan and Germany, while U.S. research support has been sporadic. The development in the past 10 years of high-temperature superconductors may alter the economics of high-speed ground transportation for the better. The goal of this work has been to design and test a novel prototype electrodynamic magnetic suspension using high-temperature superconductors and an iron core.

[1] Formerly from the Laboratory for Electromagnetic and Electronic Systems, Massachusetts Institute of Technology, Cambridge, MA 02139

ElectroDynamic magnetic suspension, called EDS Maglev and referred to as repulsive Maglev because it relies on repulsive magnetic forces, has the capability of allowing high speed transportation with a relatively large gap between the vehicle and guideway. In 1966 Danby and Powell proposed an EDS system using superconducting magnets with a "null flux" suspension that offered reduced magnetic drag. Subsequent researchers in the U.S., Japan, Germany, UK and Canada have developed further innovations, but there are still a number of technical problems that need resolution.

To date the only commercial Maglev implementations have used the electromagnetic suspension (EMS) in which electromagnets support a vehicle with attractive forces to steel guideways. While EMS may be a preferred option for lower speed designs, it has the fundamental disadvantage of requiring a small gap between the vehicle and guideway, typically less than a centimeter, and requires active control to maintain the gap. The promise of EDS is that this gap can be increased by a factor of 5 or more, and therefore guideway tolerances are relaxed and cost might be reduced. Another purported advantage of EDS is that it can be inherently stable and not dependent on feedback control to maintain a constant gap. Unfortunately, this advantage is not as real as it appears because all EDS designs are highly underdamped and, in certain cases, even unstable. Other disadvantages of EDS are higher power requirements for suspension, higher external magnetic fields, and the need for a separate low speed suspension.

The foremost problem for all high speed ground transportation systems is the high cost of guideway construction, but this key issue is not unique to Maglev. Many researchers are now convinced that if Maglev technology were fully developed it would be less expensive than a high speed train if all installation and operating costs are compared. This is particularly true if the Maglev system can provide shorter travel times which in turn attracts more users so that the capital cost per user is reduced. The reason for the EMS preference has been its apparently lower cost because it uses a relatively simpler technology with fewer unknowns. German Maglev developers have shown that EMS can operate successfully at speeds over 400 km/hour, so the problem is to improve EDS to the point that, for high speed travel, it has substantial advantages other than that of a larger gap.

We believe that a successful EDS design must face squarely the following problems:

- The cost of manufacturing and installing suspension and propulsion components on the guideway must be reduced to an absolute minimum;
- The suspension system must have a power loss that is comparable to that for EMS;
- All EDS suspension designs are highly underdamped and it is imperative to find practical means to damp oscillations and provide high ride quality;
- External magnetic fields associated with onboard superconducting magnets must be reduced particularly in the passenger compartments;
- It is highly desirable to eliminate the need for a separate low speed suspension system because this adds to the cost, weight and complexity of both the vehicle and guideway;
- Any superconducting vehicle magnets must be able to operate reliably in a hostile transportation environment.

This and two other companion papers in these *Proceedings* report the latest results of MIT research to develop an improved EDS design that addresses all of these issues.

SYSTEM OVERVIEW

This section describes the design and modeling of the multiple-loop guideway and development of circuit models to predict behavior of a full-scale flux-canceling Maglev system based on high-temperature superconducting coils. The guideway is composed of multiple conductive copper coils arranged vertically, and the train magnets are arranged in a dual-row N-S-N-S arrangement (*Fig. 1a*). The magnets in the test facility have a pole pitch $p = 0.126$ meter. When the train is in the vertical null position at $z = z_o$ and traveling in the $+y$ direction, there is no net flux through the levitating coils, and no net current induced around the loop. However, if the train's vertical position deviates from equilibrium, the net changing flux through the loop induces currents in the loop. The Lorentz force is a restoring force in this structure, with the magnetic suspension acting as a linear spring with spring constant k_z. The suspension behaves like a mass and a linear spring, with a resulting resonant frequency $\sqrt{k_z / M}$ where k_z is the magnetic spring constant and M is the total suspended mass.

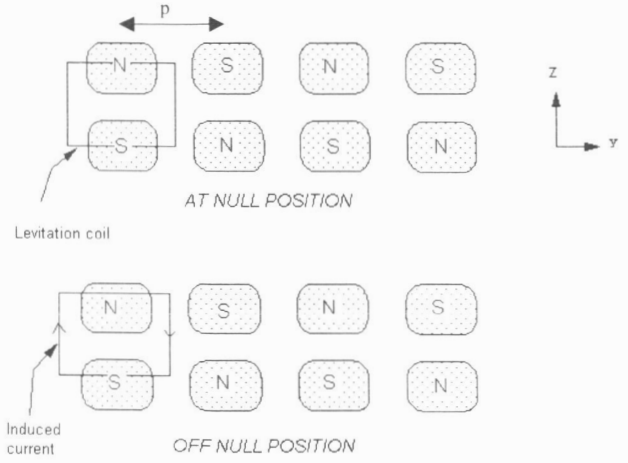

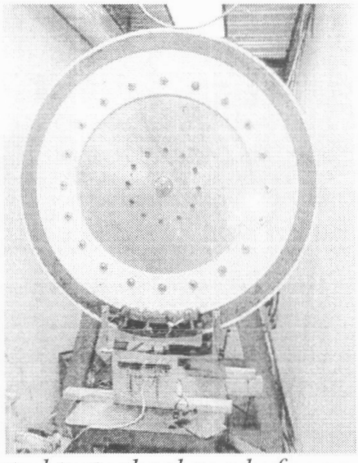

(b) Completed test wheel ready for operation

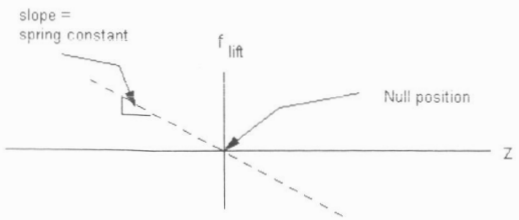

(a) Top: train at null position, no induced currents. Middle: train above null position. Currents are induced, creating a restoring force. Bottom: magnetic spring constant

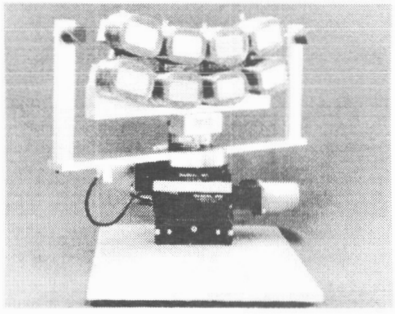

(c) Iron-core magnet, mounted to multi-axis force sensor, showing capacitive position sensors

Fig. 1. Flux-canceling Maglev topology

Guideway Coil Implementation

The guideway coils are constructed out of sheets of 0.093" thick copper, with the conductor pattern cut with a water jet and the resultant layers brazed (*Fig. 2a*). The two layers were insulated by a thin layer of non-conductive paint. The induced current path is around the thin loops on the top

layer, through the brazed rim, and around the thin loop in the bottom layer. Therefore, the electrical integrity of the rim has a large effect on the efficient operation of the guideway.

Circuit Models and Scaling Laws

Simple models may be used to demonstrate the effects of mutual coupling between guideway loops on the Maglev forces and drag peak velocity. Using a 3-coil model (*Fig. 2c*), the transfer ratio between loop current and voltage in the sinusoidal steady state is:

$$sL\begin{bmatrix} 1 & k_{12} & k_{13} \\ k_{12} & 1 & k_{12} \\ k_{13} & k_{12} & 1 \end{bmatrix} + R\begin{bmatrix} 1 & r_{12} & r_{13} \\ r_{12} & 1 & r_{12} \\ r_{13} & r_{12} & 1 \end{bmatrix} = \begin{Bmatrix} v_1 \\ v_2 \\ v_3 \end{Bmatrix} \qquad [1.]$$

The self inductance of each loop is L and the loop-loop mutual inductance $M_{ij} = k_{ij}L$ where k_{ij} is the loop coupling coefficient which is less than 1. The effects of mutual resistance are modeled by the off-diagonal term r_{ij}. The natural frequencies and mode shapes of this structure are found by solving the resultant Eigenvalue problem.

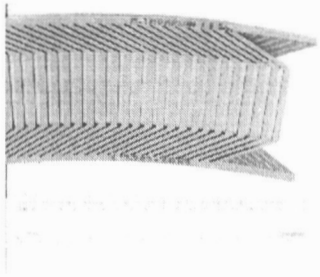

(a) Prototype guideway section showing two copper layers bolted and brazed along the edge

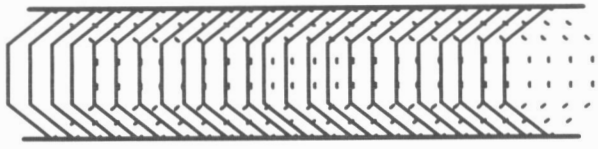

(b) Linearized geometry of guideway coils

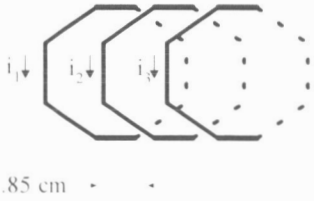

(c) Broken up into individual coils (exploded view)

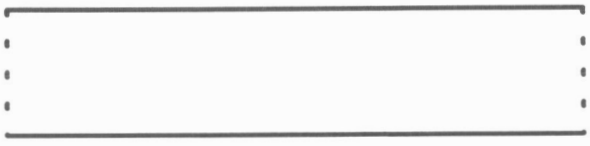

(d) Rim

Fig. 2. Guideway geometry and modeling

For the purposes of calculating guideway coil self and mutual inductances to fill the inductance matrix, approximate models were developed for this guideway structure. Although the inductances can be calculated by finite element analysis, this method gives little insight into scaling laws. Therefore, simple approximations were developed which may be used as a practical design tool.

Known solutions exist for inductor geometries such as disk coils and filamentary loops. A realizable geometry for which tabulated results exist is the round loop with rectangular cross section,

with mean radius a, axial thickness b, and trace width c (*Fig. 3a*). The self-inductance of this loop may be calculated using techniques outlined in [Grover, pp. 94], where the inductance is found to be:

$$L = 0.1aPF \qquad [2.]$$

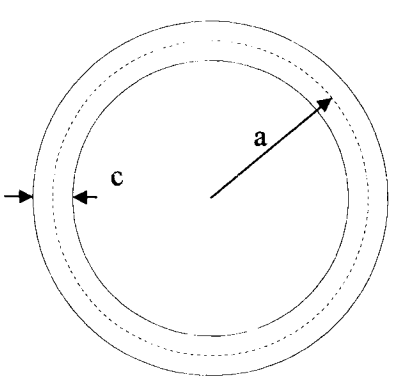

Depth b into paper

(a) Top view of disk coil

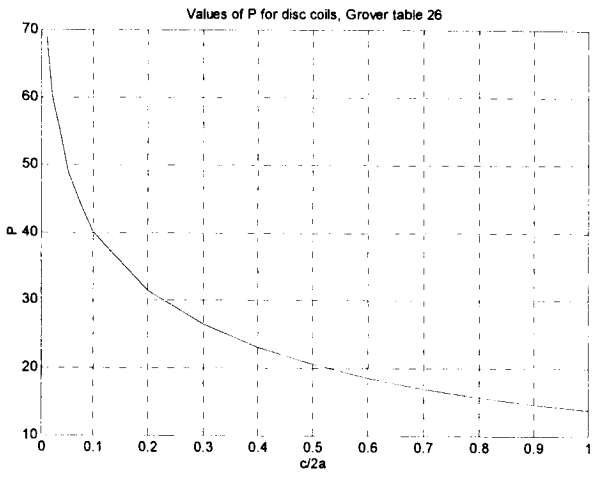

(b) Function P, for disk coils

Fig. 3. Modeling of circular coil with rectangular cross section

For this calculation, a is in meters and L is in μH. P is a function of the coil normalized radial thickness $c/2a$ (*Fig. 3b*) and applies to a coil of zero axial thickness ($b = 0$), and F accounts for the finite axial length of the coil. For $b << c$ and $c << a$ (coils resembling thin disks) the factor $F \approx 1$, an important limiting case. Therefore, for a coil with double the mean radius, there will be a corresponding doubling of the inductance.

The goal of this exercise is to approximate the complicated guideway loop geometry by a geometry where analytic expressions are available. The calculation for the circular disk coil with rectangular cross section was applied to a single loop of the guideway. Shown in *Fig. 4a* is the actual geometry of one guideway loop coil which spans one pole pitch $p = 12.6$ cm. The procedure for finding an approximate equivalent disk coil (*Fig. 4b*) is as follows:

• Calculate the circumference of the actual coil, using the mean distance to each coil element from the center	$l_{total} = 36.1$ cm
• Find the mean radius of a circular coil which has the same perimeter	$a = 5.75$ cm
• Calculate the mean radial thickness of the coil	$c = 0.39$ cm
• Find P as a function of $c/2a = 0.0337$, interpolating from Grover Table 26, pp. 113	$P = 53.87$
• Find F as a function of $c/2a$ and $b/c = 0.6082$, using Grover Table 24, pp. 108	$F = 0.9182$

This methodology is designed to match the self-inductance of the actual guideway coil with a circular coil. Results (*Table 1*) show good agreement between measurements made using an actual coil, finite element analysis on the coil, and the approximate calculation.

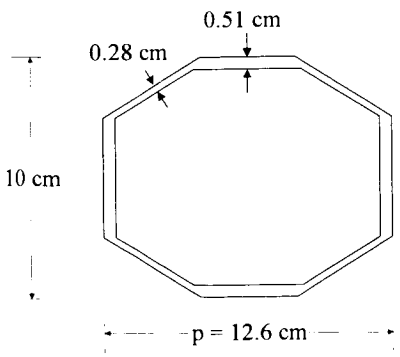

(a) Actual linearized geometry of one pole-pitch wide primitive guideway loop

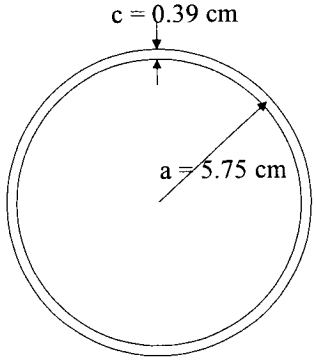

(b) Approximate model, using disk coil enclosing same perimeter

Fig. 4. Coil model, showing primative coil section and disk coil used for modeling

Table 1. Comparison of calculations on coil geometries

Measured inductance @ 10 kHz	***Grover Calculation (using circular disk coil)***	***Finite Element Analysis (using actual guideway coil geometry)***
259 nH	276 nH (see above)	280 nH

In order to calculate the mutual inductance between coils, further approximations were made by modeling the circular disk coil by a thin filament near the center of the cross-section of the disk. An approximate formula for the calculation of the self-inductance of a filamentary loop was first given by J.C. Maxwell [Maxwell, pp. 342], where:

$$L = \mu_o a\left\{\ln\left(\frac{8a}{r}\right) - 2\right\} \qquad [3.]$$

where a is the radius of the loop in meters and r is the radius of the wire. A paper by T. R. Lyle in 1913 shows that the filament approximation will give the self-inductance of any circular coil with rectangular cross section to any degree of accuracy when the mean coil radius is substituted for a and the geometric mean distance (G.M.D.) is substituted for r. The values of mean radius and G.M.D. are adjusted depending on the mean radius and the cross-section profile of the coil. The same reasoning can be applied to find the mutual inductance between filamentary loops, as in the early papers by S. Butterworth and A. Campbell. Using these approximation methods, the resultant self and mutual inductances were found (*Fig. 5*) and used to fill a 15×15 inductance matrix. The self and mutual resistances for the 15 loops was calculated and the resistance matrix was filled. These matrices were used to calculated forces, dominant time constants, and the drag peak velocity with results described later in this paper.

Once the inductance and resistance matrices are found and solved, the vectors corresponding to loop currents are used to calculate lift and drag forces. Lift force is found by:

$$< f_z(\omega) > = \frac{l}{2} \sum_{j=1}^{15} \mathrm{Re}\left\{ i_j(j\omega) B_j^*(j\omega) \right\} \qquad [4.]$$

where l is a length scale associated with the horizontal length of the coil, i_j is the induced current in the jth coil, and B_j is the average field acting on the induced current. The drag force is found by evaluating the power dissipated in the guideway coils, or:

$$< f_x(v) > = \sum_{j=1}^{15} \frac{|i_j|^2}{2Rv} \qquad [5.]$$

where v is linear velocity and R is the loop resistance.

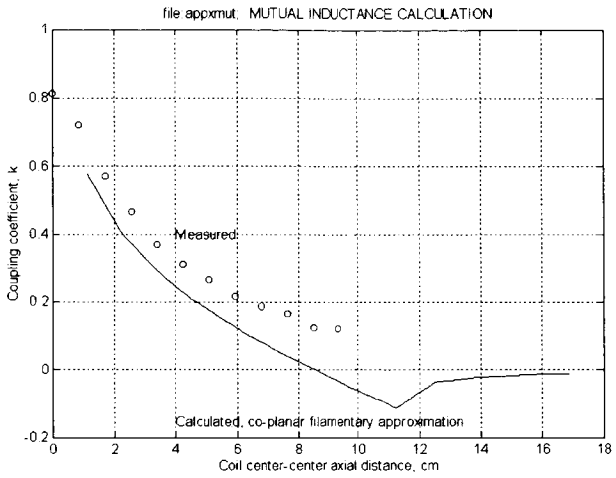

Fig. 5. Comparison of calculated (solid line) to measured guideway coil-coil mutual inductance Mutual inductance calculation based on approximations in [Butterworth]

MAGLEV TEST PROGRAM AND TEST RESULTS

Details of the test fixture including speed control of the test wheel and operation of the data acquisition system are discussed in [Kondoleon, et. al., 1995] and a companion paper in these *Proceedings*. The goals of the test program were to:

- Measure forces and moments for the magnets in different equilibrium positions and for different linear velocities using a force sensor.
- Test the viability of using AC excitation of the magnet coils to achieve significant lift force at zero train velocity.
- Test the viability of actively controlled high temperature superconducting magnets in a magnetic secondary suspension by testing the magnet with copper coils and a low-friction air bearing.

Basic Maglev Tests using Force Sensor

The result of several test wheel runs is shown in *Fig. 6*. In *Fig. 6a*, the magnet was set below the null position, and a positive lift force is measured. In *Fig. 6b*, the magnet was set +1.25 cm above the null position and a negative lift force is measured. The drag force shows a peak at approximately 20-25 meters/second. Also of note is the guidance force, which is a significant fraction of the lift

force. In *Fig. 6c*, the magnet was set near the null position, and the lift and drag forces are minimized accordingly.

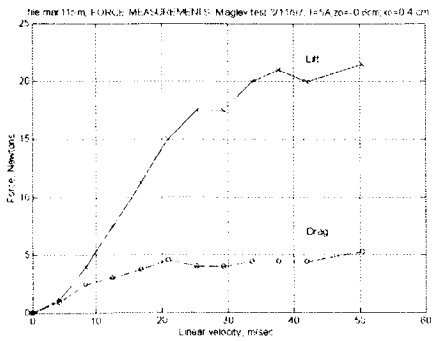

(a) Magnet below null position at z = -0.4 cm

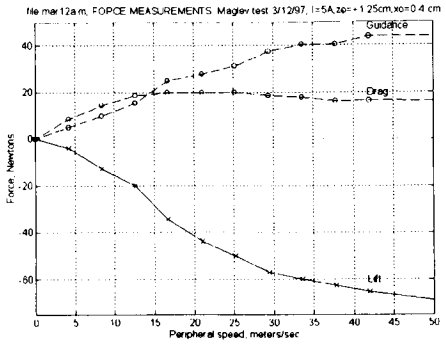

(b) Magnet above null position at z = 1.45 cm

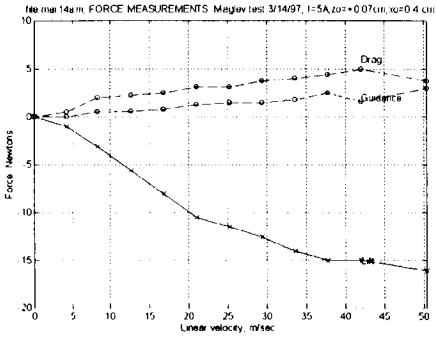

(c) Magnet slightly above null position at z = 0.27 cm

Fig. 6. Lift, drag, and guidance force measurements. I = 5A per coil, NI = 2,750 A-turns per coil, all 8 coils energized

The important results from this test are that the drag peak velocity is approximately 20-25 meters per second, which is significantly lower than the maximum test wheel speed. Therefore, data has been taken at speed significantly higher than the drag peak velocity. This critical velocity will decrease significantly for a full-scale Maglev magnet. The dependence of drag peak velocity with magnet size can be predicted with scaling laws developed later in this paper. Also, the guidance force for this configuration is a significant fraction of the lift force. This may enable a design without additional guidance coils.

The result of a calculation based on the electrodynamic model described previously is shown in *Fig. 7*, and compared to measured data taken with the test wheel in the range 0 - 600 RPM (0 - 50 meters/second). There is good agreement for the 15-coil model for the lift force f_z and the drag force f_y. The simple circuit model predicts a drag peak velocity of approximately 15 meters/second, while the measured drag peak is approximately 20-25 meters/second. The accuracy of the drag force can be further improved by accounting for parasitic eddy currents in the guideway rim, effects that are not considered by the circuit model.

Referring to *Fig. 7*, the excitation vector (top left) is approximately a half-sinusoid, corresponding to the applied magnetic field integrated over the area of the guideway loops. The

shape of this vector insures that only first and second modes will be excited, due to the orthogonality of natural modes. Measurements on drag force (bottom right) bear this out, as the measured drag peak velocity was approximately 25 meters/second and the electrodynamic model predicts ~40 meters/second. Higher-order modes are at significantly higher natural frequencies.

The lift force model shows good agreement with experiment in the 0-50 meter/second range, although there is divergence at higher velocities. This may be due to the effects of higher-order modes at higher frequencies, but further study is warranted.

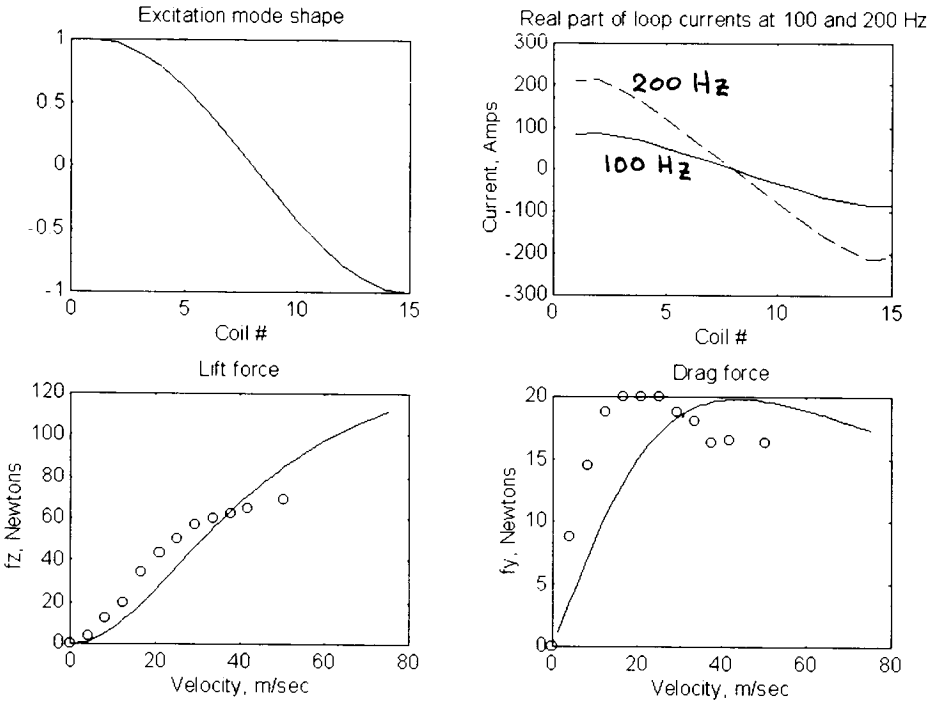

Fig. 7. Predictions of electrodynamic model with magnet +1.25 cm above null position Upper left, coil excitation vector {v}; Upper right, induced loop currents {I} at 100 Hz and 200 Hz Lower left, comparison of measured to calculated lift force vs. velocity; Lower right, comparison of measured and calculated drag force vs. velocity

Use of Scaling Laws for Full-Scale System

The goal of this section is to predict performance of a full-scale Maglev system based on scaling laws, simple guideway coil geometries, and test results from the 1/5 scale-model magnet. Results may be extrapolated from calculations on simple resistance-inductance circuits, as the previously mentioned measurements have proven this approximate technique to be valid. It is assumed that in scaling up the system, every linear dimension in the guideway and magnet is scaled by the factor ℓ.

As shown previously, the inductance of a disk inductor has the form:

$$L \propto aPF \qquad [6.]$$

where a is the mean coil radius. If all dimensions of the inductor are scaled by the factor ℓ, the inductance also scales by the same factor as P and F remain constant. The self-resistance of the loop is given by:

$$R \approx \frac{2\pi a}{\sigma bc} \qquad [7.]$$

and this resistance scales as $1/\ell$. The resultant time constant of the loop (given by L/R) scales as ℓ^2, and shows that large scale inductors will be more efficient than small ones. Given this scaling, the EDS drag peak velocity is expected to scale as $1/\ell$, although the effects of parasitic eddy currents will modify this somewhat.

The number of coil turns (N) scales with the winding area, or as ℓ^2. The average guideway field scales as ℓ, due to the ℓ^2 factor increase in turns, and the ℓ increase in pole pitch. The induced voltage V_i around a guideway loop may be expressed as:

$$V_i = j\omega B_0 A \propto l^3 \qquad [8.]$$

where B_0 is the average magnetic field, and A is the area of the guideway loop. In the high-speed limit, the induced current is limited by the inductance of the coil, as:

$$I_i \approx \frac{V_i}{j\omega L} \propto l^2 \qquad [9.]$$

The lift force is due to the product of the induced current, the applied magnetic field, and the length scale, or:

$$f_z \propto I_i B_0 l \propto l^4 \qquad [10.]$$

The maximum lift force scales as ℓ^4, which also could be inferred from evaluating the magnetic pressure acting on the iron polefaces. The drag force scales as $I_i^2 R$, or as ℓ^3 and hence the lift/drag ratio at cruising speed scales as ℓ. Other parameters such as scaling of lift/drag and lift-to-weight ratio may also be inferred from the test results. A summary of the scaling laws is shown in *Table 2*.

Using these scaling laws, performance of a full-scale magnet based on copper coils and on HTSC coils operating at 40K has been predicted (*Table 3*). The extrapolation from our 1/5-scale test results to 1.0 scale copper and for copper operating at 77K is straightforward if limitations imposed by air cooling of the copper magnets are not considered. It is unlikely that the number of Ampere-turns shown for the full-scale copper magnet would be achieved in practice due to the heat transfer limitations of air or water cooling.

It is assumed that the copper coils operating at 77K have the same power dissipation as 1.0-scale copper coils operating at room temperature. Therefore, a higher coil current is possible at 77K since the conductivity of copper at liquid nitrogen temperature is only 13% of the room temperature value. This assumes that there is sufficient copper area exposed to the boiling liquid nitrogen. An

upper limitation[2] for allowable power dissipation in the copper coil is the peak nucleate boiling heat transfer flux, which for liquid nitrogen is $q_{pk} \sim 15$ Watts/cm^2 [Iwasa, pp. 113].

The performance of a silver-sheathed HTSC magnet operating at 40K is extrapolated from the copper coil results and from available data taken from tests on HTSC coils and samples of HTSC tape. The achievable current density in HTSC at 40K is much higher than that in HTSC at 77K (approximately by a factor of 2-6 from published data). For the same number of Ampere-turns, less material will be needed for the HTSC design, resulting in a lighter coil. Current HTSC tapes are available with critical current $I_c = 40$ Amperes at 77K corresponding to a critical current density significantly higher than that supported by copper at 77K. A value of $I = 100$ Amperes or higher seems reasonable for an HTSC coil design at 40K given current technology [Iwasa, 1997]. Further improvement may be made by adjusting the dimensions of the core, as the full winding area will not be needed.

The performance of the predicted 1.0-scale HTSC magnet at 40K is comparable to that of the Japanese MLU002 test vehicle, which operates with an MMF of 700 kA-turns while generating a levitating force of 196 kiloNewtons [He, et. al, pp. 7]. The advantage to the iron-core HTSC design is that less Ampere-turns and less superconducting material is needed, and there is the possibility of actively controlling the magnet currents to achieve acceptable ride quality.

Table 2. Scaling law summary for EDS Maglev scaled by factor ℓ
Primed coordinates are for the scaled-up system

Parameter	***Constitutive Relation***	***Scaling law***
Guideway loop self-inductance, L	$L \propto \ell PF$	$L' = \ell L$
Guideway loop self-resistance, R	$R \propto 1/\sigma\ell$	$R' = R/\ell$
Guideway dominant time constant, τ	$= L/R \propto 1/\ell^2$	$\tau' = \tau/\ell^2$
Effective frequency at guideway, ω		$\omega' = \omega/\ell$
Drag peak velocity		$v_{pk}' = v_{pk}/\ell$
N, turns	$\propto \ell^2$	$N' = \ell^2 N$
Average field normal to guideway, B_o	$\propto NI/\ell \propto \ell$	$B_o' = \ell B_o$
Induced guideway loop voltage, V_i	$\propto j\omega B_o \ell^2 \propto \ell^2$	$V_i' = \ell^2 V_i$
Max. induced loop current, I_i	$\propto V_i/j\omega L \propto \ell^2$	$I_i' = \ell^2 I_i$
Lift force at cruising speed, f_z	$\propto B_o I_i \ell \propto \ell^4$	$\propto B_o I_i \cdot \propto \ell^4$
Drag force at cruising speed, f_y	$\propto I_i^2 R \propto \ell^3$	$\propto I_i^2 R \propto \ell^3$
Lift/drag ratio at cruising speed	$= f_z/f_y$	$\propto \ell$

[2] Assuming that the winding has sufficient ventilation space for the liquid nitrogen to vent

Table 3. Scaling law summary applied to test data
Comparison between 1/5 scale suspension test results, 1.0-scale copper magnet operating at room temperature, 1.0 scale copper at 77K, and HTSC at 40K (Cooling weight not included)

Parameter	***1/5-scale model***	***1.0 scale copper***	***1.0 scale copper, 77K***	***HTSC @ 40K***
Guideway loop self-inductance, L	280 nH	1.4 μH	1.4 μH	1.4 μH
Guideway loop self-resistance, R	0.0007 Ω	0.00014 Ω	0.00014 Ω	0.00014 Ω
Loop time constant, τ	0.4 msec	10 msec	10 msec	10 msec
Levitation coil turns, N	550 turns	13750	13750	1500
Levitating coil operating current, I	5 Amps	5	14.4	136[1]
Levitation power dissipation	680 Watts	85 kW	85 kW	0
NI, each coil	2750 A-turn	68750	198,450	198,450
Current density in winding, λJ	275 A/cm^2	275	800	7500
Average field normal to guideway, B_o	0.067 Tesla	0.335	0.96	0.96
Lift force at v = 100 m/s, f_z	70 Newtons	43.8 kN	365 kN	365 kN
Drag force at drag peak, f_y	20 Newtons	2.5 kN	20.8 kN	20.8 kN
Drag peak velocity v_{pk}	25 m/sec	5 m/sec.	5 m/sec.	5 m/sec.
Drag force at v = 100 m/sec	9.4 N	249 N	2.1 kN	2.1 kN
Lift/drag ratio at v = 100 m/s	7.4	175.4	175.4	175.4
Magnet core weight	29 kg	3625	3625	3625
Coil weight	8 kg	1000	1000	106
Total magnet weight[2]	37 kg	4625	4625	3731
Magnetic drag power @ 100 m/sec	0.94 kW	24.9 kW	208 kW	208 kW
Guideway power, kW/ton of lift	120 kW/ton	5.07	5.07	5.07
Lift/weight ratio	0.19	0.97	8.0	10.0

1. Assuming HTSC tape is of same cross sectional area as 18 gauge wire; for comparison only
2. Cryostat weight not included

Results of Dynamic Tests Using Air Bearing and Control System

In another set of experiments, the magnet was mounted to an air bearing which allowed low-friction vertical motion of the magnet. The control current source was connected as in *Fig. 8a*. The advantage of driving the control current at these points is that that mutual coupling reduces the power required to change the coil currents and control the lift force.

Each of the coils was energized with 6 Amps DC by the main power supply V_m. With the air bearing energized and the control system deactivated, the vertical magnet position was perturbed approximately +1 centimeter from the equilibrium position and the resultant transient decay of magnet position was observed (*Fig. 8a*). The oscillatory behavior is at 1.15 Hz with a damping ratio of approximately 1%, corresponding to the expected underdamped EDS response.

A similar experiment was run, but with the control system operating (*Fig. 8c*). Vertical position of the magnet was measured with a frictionless LVDT and a P.I.D. controller which controlled the current source I_c. The resultant magnet vertical position response is much more

damped ($\varsigma \sim 40\%$) showing that the control system is operating correctly. Further improvement can be made in the transient response by adjusting the loop parameters.

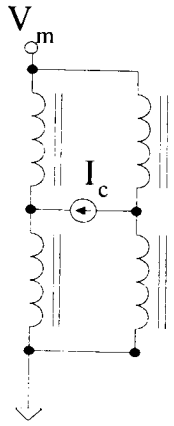

(a) Wiring

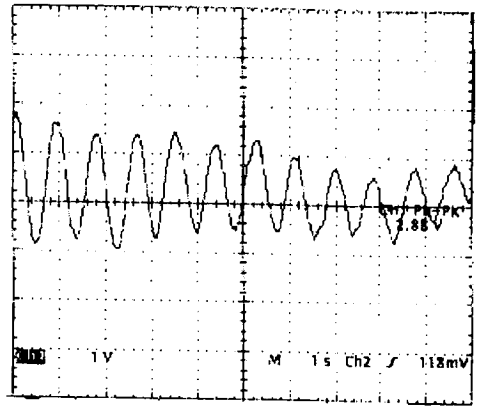

(b) Control system not activated, initial deflection 1 cm; oscillation frequency 1.15 Hz

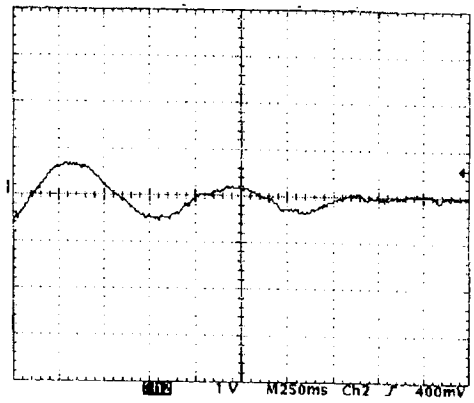

(c) Control system operational

Fig. 8. Test of vertical control system

AC Lift Measurements

Further tests were run to determine if significant lift is possible at zero train velocity by exciting the levitation coils with AC currents. Generating lift at zero velocity is desirable, as this can remove the need for a low speed suspension. The fact that high temperature superconductors are robust with regard to AC losses is a further motivation, as such control is difficult using low temperature superconductors due to quenching.

For this series of tests, the coils were wired as in *Fig. 9a*. The coils were wired so that for the first half cycle of the sinewave current excitation, the top two coils are in a North-North arrangement, and the bottom two coils are energized South-South. For this configuration, if the guideway is offset from the null position, there is a net changing flux through the guideway loops and hence a restoring force.

Results of AC lift measurements are shown in *Fig. 9b* for various equilibrium displacements from the null position, and for excitation frequencies of 10, 20, 50 and 100 Hz. A maximum frequency of 100 Hz was chosen[3] as this is the approximate equivalent frequency of the Maglev drag peak, and higher frequencies will not result in significantly higher lift. The data shows that lift comparable to that achieved by electromagnetic induction by motion can be achieved, however at the cost of high power delivery from the magnet current source. Scaling laws can be used to show that a full-scale magnet with eight coils each with $NI = 165{,}000$ (corresponding to $N = 2062$ turns and $I =$ 80 A p-p) will generate approximately 1 ton of lift with a lift-to-weight ratio of 0.28 at 100 Hz (*Table 4*). With $NI = 495{,}000$ A-turns p-p, a magnet lift-to-weight ratio of ~2.5 will be achieved for a full-scale magnet based on an HTSC coil. The primary losses will be switching losses in the driving electronics, and AC losses in the levitation and guideway coils. The actual lift-to-weight ratio will

[3] If the operating frequency is known and does not change, a series capacitor can be added to resonate with the inductive load to reduce the large reactive voltage required to drive the magnet coil.

be less due to the weight of the cooling system, and further study is required to determine the extent of power losses in the HTSC coil due to switching.

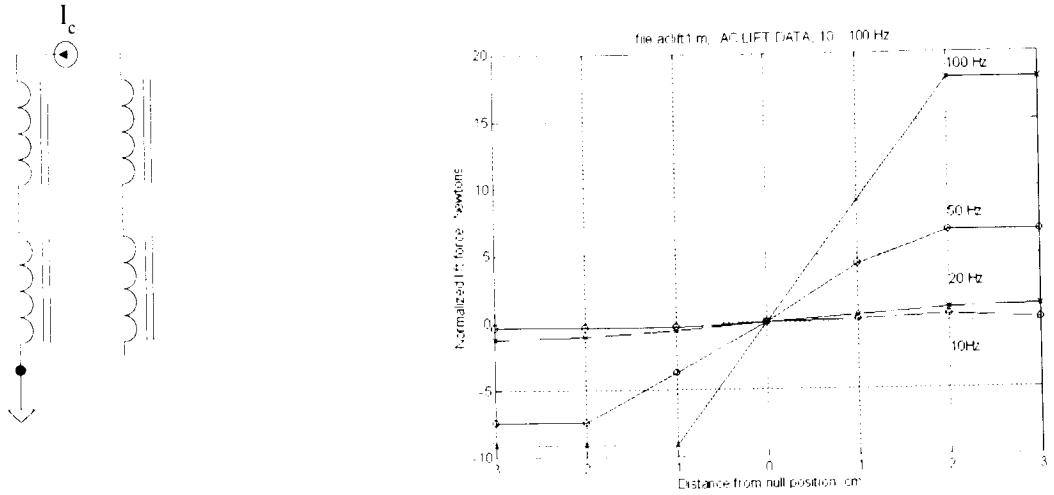

(a) Magnet wiring for AC lift measurements *(b) Test results for AC lift*

Fig. 9. AC lift measurements at 10, 20, 50 and 100 Hz

Table 4. Scaling laws applied to AC lift measurements (Cryostat weight not included)

	1/5-scale copper, I = 12A, 100 Hz	***1.0 scale HTSC @ 40K, I=80A p-p, 100 Hz***	***1.0 scale HTSC @ 40K, I=240A p-p, 100 Hz***
Ampere turns, p-p	6,600	165,000	495,000
Lift force	17 N	10625 N	95,625 N
Lift/weight ratio	0.05	0.28	2.5

CONCLUSIONS

Results from these series of Maglev tests show that there is good agreement between predictions based on simple circuit models with measurements taken on the test fixture for lift force, drag force, and magnetic drag peak. The models could be improved by doing additional finite-element analyses and extending the 15-coil model so that the infinitely long guideway is better approximated.

The use of an iron core offers significant advantages such as rapid attenuation of the far magnetic field. Furthermore, the iron core reduces the mass of superconducting material needed for a given guideway field. The iron can be used to reduce the magnetic field impinging on the coils so that the critical current is maximized.

Vertical force can be controlled by differential control of the magnet currents. Vertical position can be actively damped by utilizing an active magnetic secondary suspension. Use of HTSC may overcome the limitations imposed by mechanical secondary suspensions. The guidance force

measured was a significant fraction of the lift force. Similar reasoning could be used to design a guidance system, for horizontal train control, based on flux-canceling concepts.

It is possible to generate lift with AC currents using this configuration. The robustness of HTSC with regard to AC losses may make AC lift a viable alternative to low-speed mechanical suspensions. However, cooling requirements will probably limit the duration for which AC lift may be operated. Scaling laws were derived which show that the performance of an HTSC-based design at 40K may be comparable to that of low-temperature superconducting designs, with the advantage of less weight and the possibility of using AC lift for low-speed suspension.

ACKNOWLEDGMENTS

Thanks are due to the U.S. Department of Transportation, Federal Railroad Administration, through the Volpe National Transportation Systems Center, Cambridge, MA, which funded this work.

REFERENCES

[1] S. Butterworth, "On the Coefficients of Self and Mutual Induction of Coaxial Coils," *Philosophical Magazine*, vol.29, 1915, pp. 578-592

[2] S. Butterworth, "On the Coefficients of Mutual Induction of Eccentric Coils," *Philosophical Magazine*, series 6, vol.31, 1916, pp. 443-454

[3] A. Campbell, "On the Use of Variable Mutual Inductances," *Philosophical Magazine*, vol. 15, 6th series, 1908, pp. 155-171

[4] F. W. Grover, *Inductance Calculations: Working Formulas and Tables*, Dover Publications, Inc., New York, 1946

[5] J. L. He, D. M. Rote, and H. T. Coffey, "Study of Japanese Electrodynamic-Suspension Maglev Systems," *Argonne National Laboratory report ANL/ESD-20*, April 1994

[6] Y. Iwasa, *Case Studies in Superconducting Magnets*, pub. by Plenum Press, New York, 1994

[7] Y. Iwasa, personal communication, 1997

[8] A. Kondoleon, D. Seltzer, R. D. Thornton, and M. T. Thompson, "Development of a Large Scale High Speed Wheel Test Facility," *Proceedings of the Third International Symposium on Magnetic Suspension Technology*, NASA Conference Publication 3336, part 2, pp. 523-534, Dec. 13-15, 1995

[9] T. R. Lyle, "On the Self-Inductance of Circular Coils of Rectangular Section," *Philosophical Transactions*, vol. 213A, (1913) pp. 421-435

[10] J. C. Maxwell, *A Treatise on Electricity and Magnetism*, vols. 1 and 2, Dover Publications

[11] M. T. Thompson, "High Temperature Superconducting Magnetic Suspension for Maglev," Ph.D. Thesis, Department of Electrical Engineering and Computer Science, Massachusetts Institute of Technology, May 1997

[12] M. T. Thompson and A. Kondoleon, "Test Results from a Large Scale, High Speed EDS MAGLEV Wheel Test Facility," these *Proceedings*

[13] R. D. Thornton, D. Perreault, T. Clark, "Linear Synchronous Motors for Maglev," *U.S. Dept. of Transportation, Federal Railroad Administration Report DOT/FRA/NMI-92/13*, January 1993

[14] R. D. Thornton and M. T. Thompson, "Magnetically Based Ride Quality Control for an Electrodynamic Maglev Suspension," these *Proceedings*